Journal of Molecular Liquids 435 (2025) 128035

Contents lists available at ScienceDirect

Journal of Molecular Liquids

journal homepage: www.elsevier.com/locate/molliq

Extending the Madrid-2019 force field to the perchlorate anion: Role of charge distribution and validation with experiments on Mars-relevant aqueous solutions

S. Blazquez [a], J. Troncoso [b], P. La Francesca [c], P. Gallo [c], M.M. Conde [d], C. Vega [a,*]

[a] Departamento de Química Física, Facultad de Ciencias Químicas, Universidad Complutense de Madrid, 28040 Madrid, Spain
[b] Departamento de Física Aplicada, Universidade de Vigo, Escola de Enxeñaría Aeronaútica e do Espazo, E 32004, Ourense, Spain
[c] Dipartimento di Matematica e Fisica, Università degli studi Roma Tre, via della Vasca Navale 84, Roma, 00146, Italy
[d] Departamento de Ingeniería Química Industrial y del Medio Ambiente, Escuela Técnica Superior de Ingenieros Industriales, Universidad Politécnica de Madrid, 28006, Madrid, Spain

ABSTRACT

The perchlorate anion (ClO_4^-) has garnered increasing interest in recent years due to its presence on Martian soil (and subsoil). In this study, we extend the Madrid-2019 force field (which uses a scaled charge of ±0.85*e* for monovalent ions and the TIP4P/2005 model for water) to the perchlorate anion. We propose two models with identical Lennard-Jones parameters but different charge distributions (i.e., the total charge of the anion is -0.85 in both models, but the partial charges assigned to the Cl and O atoms differ in each model). The experimental densities of several soluble perchlorate salts (i.e., $LiClO_4$, $NaClO_4$, $KClO_4$, $Mg(ClO_4)_2$ and $Ca(ClO_4)_2$) are well described up to the solubility limit of each salt with both force fields. The viscosity of $Mg(ClO_4)_2$ and $Ca(ClO_4)_2$ solutions at 298.15 K and room pressure was also determined experimentally. The transport properties show differences due to the charge distribution; specifically, the model with a greater difference in partial charges between the ions is less viscous (thus exhibiting higher diffusion) and aligns more closely with experimental results. We also performed experimental measurements of density at ambient pressure as a function of temperature for supercooled $Mg(ClO_4)_2$ and $Ca(ClO_4)_2$ solutions and compared them against simulation results to locate the temperature at which the maximum in density occurs (TMD). The two models agree well with the experimental results although the exact location of the TMD is sensitive to the internal charge distribution within the perchlorate anion. Additionally, structural features of perchlorate solutions were calculated, finding negligible differences between the proposed models. Finally, we tested the possibility of combining the Madrid-2019 force field with the TIP4P/Ice model of water showing also excellent predictions of the experimental densities.

1. Introduction

The perchlorate anion is of great importance due to its unique chemical properties and potential implications for extraterrestrial habitability. One of the most fascinating discoveries of the Phoenix Mission to Mars in 2008 was the detection of perchlorate salts in Martian soil mixed with water in the North Polar region of the planet [1–9]. Perchlorates are highly soluble salts capable of significantly lowering the freezing point of water. Regarding the salts found on Mars, $Mg(ClO_4)_2$ and $Ca(ClO_4)_2$, their eutectic temperatures are -57 °C and -74.4 °C, respectively [10,11]. This remarkable decrease suggests that liquid saline water or brines could have existed on Mars [12,13], particularly in areas disturbed by the Phoenix Lander, fulfilling key criteria for potential habitability. Furthermore, recent experimental observations have been interpreted as indicating the presence of aqueous solutions about 1.5 km underneath the Martian south pole [14,15]. Thus, the properties of supercooled aqueous perchlorate solutions, such as the temperature of maximum density (TMD), are of great interest. However, to the best of our knowledge, no experimental studies have been conducted on these systems, although recent simulations have explored them [16,17].

Besides, perchlorate is a dangerous pollutant [18–22]. Industrial and military operations use ammonium perchlorate as a fuel in rockets [23], and in some cases, it is also found in fertilizers [24]. Most perchlorate salts have high water solubility, and once dissolved, perchlorate becomes extremely mobile, taking decades to degrade. The health effects of ingesting low doses of perchlorate-contaminated water are not well understood. However, it is known to interfere with the body's iodine intake, inhibiting thyroid hormone production [25–27] since the ClO_4^- ion is similar to iodine in both charge and ionic radius.

As mentioned, one of the main interests in perchlorate salts arises from their presence on the soil and subsoil of Mars, where extremely low temperatures are reached [28]. In this context, simulations repre-

* Corresponding author.
E-mail address: cvega@ucm.es (C. Vega).

https://doi.org/10.1016/j.molliq.2025.128035
Received 28 March 2025; Received in revised form 10 June 2025; Accepted 23 June 2025
Available online 30 June 2025

sent a powerful tool for studying these extreme conditions [16,17,29]. However, to accurately simulate aqueous solutions of perchlorate salts, a suitable force field is required. Several models are available to simulate this anion [30–36]. Nevertheless, in recent years, the methodology and approach to develop force fields with scaled charges for ions have demonstrated excellent accuracy in describing aqueous electrolyte solutions [37–56]. Therefore, it is of interest to extend this approach to model the perchlorate anion.

The use of scaled charges was first proposed by Leontyev and Stuchebrukhov and was denoted as Electronic Continuum Correction (ECC) [57–60]. In their work, they argued that the dielectric constant of non-polarizable models at high frequencies (ε_∞) was 1, whereas for water, it was 1.78. They proposed applying a factor $q_{scaled} = 1/\sqrt{\varepsilon_\infty}$ to the ions leading to a $q_{scaled} = 0.75e$. Nevertheless, another reasoning was proposed by Kann and Skinner [61] which also leads to a scaled charge for the ions. In this case, they suggested that the Coulombic energy between ions at infinite dilution and infinitely large distances should be the same for experiment and simulation (i.e., recovering the Debye–Huckel law). By employing this approach, the charge of the ions depends on the value of the dielectric constant of the model. Thus, in the case of the TIP4P/2005 water, the dielectric constant is about 57, leading to a value of $\pm 0.85e$ for the ions.

Anyway, both approaches lead to scaled charges, which is a way of incorporating a kind of polarizability into the system and also accounts for the charge transfer that occurs between ions and surrounding water molecules in solution [62,63]. As previously mentioned, many properties of aqueous solutions are well described using scaled charges. However, there is no a unique scaled charge value that accurately describes all properties, as we have recently shown [64]. Although a scaled charge of $\pm 0.85e$ can serve as a compromise where most properties are reasonably well described, transport properties, for example, are better captured with a lower scaled charge of $\pm 0.75e$. Interestingly, in the case of polyatomic ions, we have observed that viscosities are well described -or even underestimated- when using a total charge of $\pm 0.85e$ for the ion. This behavior has been observed in SO_4^{2-} [65], $B(OH)_4^-$ [55], NO_3^- [66], and NH_4^+ [66]. We hypothesize that this difference arises from the charge distribution within the molecule (i.e., the partial charges assigned to each atom), which represents an additional degree of freedom not present in monatomic ions. In fact, we recently developed two force fields for the OH^- ion, both with the same net charge (-0.85e) but different partial charge distributions, and we observed noticeable differences in certain properties [53,67]. In fact, the role of the internal charge distribution was also studied by McFegan et al. [68] in tetramethylammonium iodide solutions, addressing the surface tension of the solutions. Hence, it is of significance to further investigate the effect of charge distribution in more complex polyatomic ions such as ClO_4^-.

In this work, we develop a force field for the perchlorate anion (ClO_4^-), assigning a total scaled charge of $-0.85e$ while employing two different partial charge distributions to study the effect of charge distribution. First, we adjust the model to fit the experimental densities of five soluble perchlorate salts, namely $LiClO_4$, $NaClO_4$, $KClO_4$, $Mg(ClO_4)_2$, and $Ca(ClO_4)_2$. Then, we study several properties of interest, such as viscosities, diffusion coefficients, temperatures of maximum density (where experimental measurements have been performed), and structural features. Finally, we evaluate the compatibility of this force field with the TIP4P/Ice water model.

2. Simulation details

We have performed Molecular Dynamics (MD) simulations using the GROMACS package (version 4.6.5) [69,70]. We used the leap-frog integrator algorithm [71] with a time step of 2 fs. Periodic boundary conditions have been employed in all the xyz directions. Temperature and pressure were kept constant by employing the Nosé-Hoover thermostat [72,73] and the Parrinello-Rahman barostat [74], respectively, both with time constants of 2 ps. The cutoff radius employed for van der Waals and electrostatic interactions was 1.0 nm. Long-range energy and pressure corrections were also applied to the LJ part of the potential. The smooth PME method [75] is used to account for the long-range electrostatic forces. To maintain the geometry of the molecules we used the SHAKE algorithm [76]. The interaction parameters for the counterions (*i.e.*, Li^+, Na^+, K^+, Mg^{2+}, Ca^{2+}) were obtained from the Madrid–2019 force field [65–67,77,78], while those of the TIP4P/2005 model are taken from Ref. [79]. In the Madrid-2019 force field the interaction between ions and ions and water has two different contributions. The first one is an electrostatic (coulombic) contribution and the second one a van der Waals interaction represented by the LJ potential so that the interaction between atom/site i and atom/site j is described as:

$$u(r_{ij}) = \frac{1}{4\pi\varepsilon_0}\frac{q_i q_j}{r_{ij}} + 4\epsilon_{ij}\left[\left(\frac{\sigma_{ij}}{r_{ij}}\right)^{12} - \left(\frac{\sigma_{ij}}{r_{ij}}\right)^{6}\right], \quad (1)$$

where, q_i is the ionic charge, ε_0 is the vacuum permittivity, ϵ_{ij} the well depth energy of the LJ potential, and σ_{ij} the LJ diameter.

To develop the force field parameters we employed a similar methodology to that employed in Refs. [65–67,77,78]. In short, we adjust the perchlorate-water interactions (deviating when needed from the Lorentz-Berthelot (LB) combining rules) to reproduce the experimental bulk densities as a function of the electrolyte molality. Mainly, we adjust the $\sigma_{O_w-O_p}$ (where O_w and O_p denote the oxygen atoms of water and perchlorate respectively) interactions through a trial-and-error procedure. Then, we adjust the densities at high concentrations (i.e., at the highest concentration studied for each salt in this work: 5 m for $LiClO_4$, 15 m for $NaClO_4$, 4 m for $Mg(ClO_4)_2$, and 7 m for $Ca(ClO_4)_2$), avoiding precipitation of the salt by fitting the cation–anion interactions if necessary. The geometry of the ClO_4^- anion (i.e., $\widehat{O_pClO_p}$ angle of 109.5° and O_p–Cl_p distance of 1.43 Å) was fixed according to experimental results [80,81] (where Cl_p denotes the chlorine atom of the perchlorate anion). We have modeled perchlorate setting four interacting sites at the positions of the oxygen atoms in a tetrahedral arrangement and a massless interacting site located on the chloride atom. Details about how to implement this geometry in MD programs are provided in the Appendix. All the results of this work were obtained with a Rigid version of the perchlorate anion but in the Appendix A, a Flexible version of the force field of this work is also presented and discussed. The optimized potential parameters and charges for perchlorate are collected in Tables I and II.

Densities, radial distribution functions (RDFs) and diffusion coefficients were obtained by simulating in the NpT ensemble a system comprised of 555 water molecules and the corresponding number of ions needed to achieve the desired molality over ~50 ns.

Table I
Summary of the force field parameters for the Lennard-Jones (σ_{ii} and ε_{ii} are taken from Ref. [30]) and Coulombic (atomic charges, q_i) contributions to the pair potential for the perchlorate anion developed in this work. The geometry of the ClO_4^- ion is defined by a $\widehat{O_pClO_p}$ angle of 109.5° and a O_p–Cl_p distance of 1.43 Å, being O_p and Cl_p the oxygen and chloride atoms of the perchlorate anion respectively. The O_p-O_p distance is 2.335 Å. Both models A and B perform quite well, but model A provides a better description of the transport properties.

Model A

ClO_4^-	σ_{ii} (Å)	ε_{ii} (kJ·mol^{-1})	q (e)
Cl_p	3.47094	1.108760	+0.3500
O_p	2.95992	0.878640	–0.3000

Model B

ClO_4^-	σ_{ii} (Å)	ε_{ii} (kJ·mol^{-1})	q (e)
Cl_p	3.47094	1.108760	+0.0000
O_p	2.95992	0.878640	–0.2125

Table II
Lennard-Jones σ_{ij} (in Å) and ε_{ij} (in kJ/mol) parameters between perchlorate anion and ions developed in this work. O_p and Cl_p are the oxygen and chloride atoms of the perchlorate anion respectively. LJ parameters are the same for both models A and B. Parameters for TIP4P/2005 water were taken from Ref. [79]. LJ parameters for the self- and crossed-interaction between Li^+, Na^+, Mg^{2+} and Ca^{2+} are taken from the Madrid–2019 force field [65–67,77,78]. In cases where a numerical value is not given, the Lorentz-Berthelot (LB) combination rules were followed, as indicated. O_w stands for the oxygen of water and O_p and Cl_p represent the oxygen and chloride atoms of the perchlorate anion respectively.

	σ_{ij} (Å)		ε_{ij} (kJ·mol^{-1})	
Atom	Cl_p	O_p	Cl_p	O_p
O_w	LB	3.2570	LB	0.8251
Li^+	LB	LB	LB	LB
Na^+	LB	2.7000	LB	1.1374
K^+	LB	LB	LB	LB
Mg^{2+}	LB	LB	LB	LB
Ca^{2+}	LB	2.6500	LB	0.6676
Cl_p	-	LB	-	LB

For the diffusion coefficients, D, we used the Einstein relation:

$$D = \lim_{t\to\infty} \frac{1}{6t} \left\langle [\mathbf{r}_i(t) - \mathbf{r}_i(0)]^2 \right\rangle, \tag{2}$$

where $\mathbf{r}_i(t)$ and $\mathbf{r}_i(0)$ are the position of the i^{th} particle at time t and at a certain origin of time, respectively, and $\langle\cdot\rangle$ is the time average. The diffusion coefficients were then obtained, avoiding the subdiffusive regime, from the slope of the plot of the mean square displacement (MSD), given by $\langle[\mathbf{r}_i(t) - \mathbf{r}_i(0)]^2\rangle$, against time. As shown by Santos et al. [82], the diffusion coefficient D can be calculated as an average over multiple trajectories to estimate statistical uncertainties. In this work, we performed three independent simulations for the 4 m $NaClO_4$ solution, observing differences of less than $0.01\cdot10^{-9}$ m^2·s^{-1}. Therefore, we consider this value as the statistical error associated with the diffusion coefficients reported in this study. See SM for the numerical values of the diffusion coefficients of water and for the plots of MSD *vs* time (Fig. S2).

For all the results of this work we applied the hydrodynamic corrections of Yeh and Hummer [83] which are described in Eq. (3)

$$D = D_{MD} + \frac{k_B T \xi}{6\pi\eta L} \tag{3}$$

where D is the diffusion coefficient with the applied corrections of Yeh and Hummer, D_{MD} is the diffusion coefficient initially obtained by simulations, ξ is a constant (its value is 2.837), L is the length of the simulation box and η is the viscosity of the solution at the studied concentration. We have used the experimental viscosities of $NaClO_4$ and $Mg(ClO_4)_2$ solutions to correct their respective diffusion coefficients. On the other hand, due to the lack of experimental viscosity data for $LiClO_4$ solutions, we have employed the viscosities of $NaClO_4$ as a proxy to correct the diffusion coefficients of this salt.

A bigger system with 4440 water molecules was employed to calculate the viscosities. To compute viscosities we followed the methodology proposed by Gonzalez and Abascal [84]. This involves, first, an equilibration of the system using an *NpT* simulation to calculate the average box volume, followed by a NVT simulation of 50 ns. From the components $P_{\alpha\beta}(t)$ of the pressure tensor we calculated the viscosity using the Green-Kubo formalism:

$$\eta = \frac{V}{k_B T} \int_0^\infty \langle P_{\alpha\beta}(t_0 + \tau)\, P_{\alpha\beta}(t_0)\rangle \, d\tau, \tag{4}$$

with k_B the Boltzmann constant.

Finally, by using the system of 4440 molecules, we checked the absence of salt precipitation during 50 ns at the experimental solubility limits of each salt. The experimental values of solubility at 25 °C are collected in Table III.

Table III
Experimental salt solubility in water at 298.15 K and 1 bar in molality units as reported in Ref. [85].

Salt	Solubility (mol/kg)
$LiClO_4$	5.5
$NaClO_4$	16.7
$KClO_4$	0.15
$Mg(ClO_4)_2$	4.5
$Ca(ClO_4)_2$	7.9

3. Experimental procedure

Magnesium and calcium perchlorates were purchased from Sigma-Aldrich with a purity greater than 0.99 in mass fraction. The solutions were made using MilliQ water. They were weighed in an AE-240 Mettler Toledo balance with an uncertainty of 0.1 mg. The uncertainty in molality was estimated in 0.004 mol/kg.

Dynamic viscosity η was measured at 298.15 K using an Anton Paar AMVn falling ball viscometer, which determines it by measuring the time t it takes for a gold-plated ball to fall through a capillary filled with the sample and tilted to a preset angle:

$$\eta = K(\rho_b - \rho)t, \tag{5}$$

where K is the calibration constant, ρ_b the ball density (7.85 g·cm^{-3}), and ρ the density of the sample. K was calculated from an experiment with MilliQ water, whereas ρ was measured using a DMA 5000 densimeter from Anton Paar, calibrated with MilliQ water and octane. Uncertainty in viscosity measurements was estimated in 2%. More details on the experimental procedure can be found elsewhere [86].

Densities were measured using a pycnometer formed by a flask attached to a capillary tube. The density of the sample was determined from the height L of the meniscus in the capillary:

$$\rho = \rho_0 \frac{V_{f,0} + S_0 L_0}{V_{f,0}(1+3\delta) + S_0 L (1+2\delta)(1+\delta)}. \tag{6}$$

Here, $V_{f,0}$, S_0, and L_0 are the flask volume, the capillary cross sectional area, and the meniscus position at the reference temperature T_0, respectively, obtained by calibration experiments with pure water. The δ parameter takes into account the thermal expansion of the pycnometer, $\delta = \alpha(T - T_0)$, being α the linear thermal expansivity of the glass. ρ_0 is the density of the sample at the reference temperature, determined using the DMA 5000 densimeter. Since this procedure did not allow determining the TMD of the $Ca(ClO_4)_2$ solution at 0.4 m due to freezing, its density at temperatures below -8 °C was measured through thin capillary tubes of very small volume (approximately 0.007 mL). This prevents the freezing of the sample, so density data could be determined at lower temperatures. The equation (6) was also used to obtain the density, but with $V_{f,0} = 0$. Details about these experimental techniques can be found in Ref. [87]. Density was fitted versus temperature to a third order polynomial, and by equating the derivative to zero, the TMD is determined. Uncertainties were estimated as 0.5 kg·m^{-3} for densities, 0.3 K for the TMD of $Mg(ClO_4)_2$, and 1.5 K for the TMD of $Ca(ClO_4)_2$.

4. Results

As explained in previous sections, we have designed two different force fields for the perchlorate anion by modifying the charge distribution. The LJ parameters and the total net charge in both models are the same. The only difference lies in the partial charges assigned to each atom in the molecule. In Model A, we assign a charge of +0.35*e* to the Cl_p atom and -0.3*e* to each O_p atom. This charge distribution is based on the work of Heinje et al. [32], where they obtained these charges from

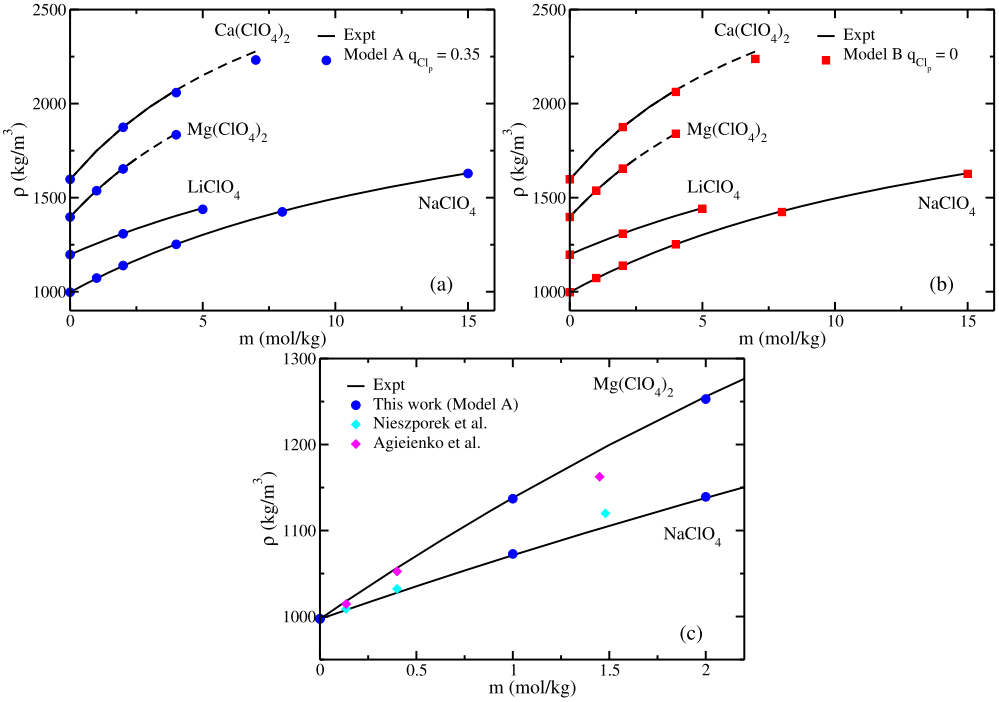

Fig. 1. Density as a function of molality at T = 298.15 K and 1 bar for different perchlorate aqueous solutions. (a) Results for model A. (b) Results for model B. Blue circles and red squares are the simulation results of this work using models A and B respectively. Solid black lines: fit of experimental data at T = 298.15 K and 1 bar taken from Ref. [89] for $LiClO_4$, from Ref. [90] for $NaClO_4$ and $Ca(ClO_4)_2$ and from Ref. [91] for $Mg(ClO_4)_2$. In (a) and (b) Results for $LiClO_4$, $Mg(ClO_4)_2$ and $Ca(ClO_4)_2$ were shifted up 200, 400 and 600 density units respectively for a better legibility. c) Comparison with other models: blue circles are the results of this work for Model A; cyan diamonds are the results with the model of Nieszporek et al. [30] for $NaClO_4$ which uses a charge of $q_{Cl_p} = 1.0786$, taken from Ref. [16]; magenta diamonds are the results with the model of Agieienko et al. [31] for $Mg(ClO_4)_2$ which uses a charge of $q_{Cl_p} = 1.309$, taken from Ref. [17].

a LCAO-MO-SCF (Linear Combination of Atomic Orbitals – Molecular Orbital – Self-Consistent Field) calculation. However, given the similar electronegativities of Cl and O (3.16 and 3.44, respectively) we propose an alternative charge distribution in which the charges assigned to these atoms are more similar. In Model B, we assign a partial charge of 0*e* to the Cl_p, while a charge of -0.2125*e* for the oxygens O_p. In any case, in both cases, the total charge assigned to the perchlorate anion is -0.85*e*.

4.1. Densities

As previously mentioned, we have adjusted the developed force field to reproduce the experimental densities of different perchlorate salts up to the solubility limit of each salt. Interestingly, the LJ parameters are the same for both models. In Fig. 1 we have plotted the experimental densities of the soluble perchlorate salt as a function of salt molality (i.e., mols of solute per kg of water). The simulation results are shown as a blue circles for model A (Fig. 1(a)) and red squares for model B (Fig. 1(b)). In both cases, it is evident that the force field is able to reproduce the experimental densities up to the solubility limit of each salt. Notice that for divalent salts (i.e., $Mg(ClO_4)_2$ and $Ca(ClO_4)_2$) some experimental results were extrapolated (dashed black lines) due to the lack of available experiments. In any case, the simulations match extraordinarily well with experiments, although a slight underestimation is observed for $Ca(ClO_4)_2$. For $KClO_4$, we have not included the results due to its low solubility (0.15 m at 25 °C). However, the experimental density [88] of this solution at 0.1 m is 1005.5 kg/m^3, while those provided by models A and B are 1006.0 kg/m^3 and 1006.1 kg/m^3, respectively, showing an excellent agreement between experiments and simulations. An interesting conclusion arises from these calculations: changing the charge distribution does not affect the density as long as the total net charge and LJ parameters remain unchanged.

Finally, Fig. 1(c) shows a comparison of our model densities (blue circles) for $NaClO_4$ and $Mg(ClO_4)_2$ solutions with other models of perchlorate. The simulation data of these force fields were taken from the works of La Francesca and Gallo [16,17], using the models proposed by Nieszporek et al. [30] for $NaClO_4$ (which assigns a charge of $q = 1.0786e$ to Cl_p) and Agieienko et al. [31] for $Mg(ClO_4)_2$ (which assigns a charge of $q = 1.309e$ to Cl_p). It can be seen that, at low concentrations, the model performs reasonably well. However, for $NaClO_4$, it starts to overestimate, and for $Mg(ClO_4)_2$, it starts to underestimate densities at around 1.5 m, performing worse than our proposed model. This also suggests that these models (which assign unit charges to the ions, in contrast to ours) would perform even worse at higher concentrations. Thus, the two proposed models in this work, with scaled charges for the ions, better reproduce the experimental densities across the entire concentration range up to the solubility limit of each salt.

4.2. Viscosities and diffusion coefficients

Once densities of perchlorate salts have been calculated, it is interesting to analyze some transport properties such as viscosities and diffusion coefficients. Starting from viscosities, we have computed them for $NaClO_4$ solutions at 2 and 4 m. In Fig. 2, we present the results for models A and B. Although both models overestimate the experimental viscosities, significant differences can be observed. Model A, which features a greater difference in charge distribution between ions, exhibits better agreement with experimental data than Model B. In contrast, Model B, with more similar partial charges for Cl and O, shows a larger overestimation of viscosities. This behavior indicates that, unlike in the case of densities, the charge distribution in a polyatomic ion plays a role in viscosity. This finding was suggested in previous works [55,65,66] and has been observed for a simpler—although not monatomic—ion such as OH^- [53,67]. Increasing the charge of the chlorine atom of the perchlorate anion from $q_{Cl_p} = 0e$ to $q_{Cl_p} = 0.35e$ decreases the viscosity and improves the agreement with experiment. One could raise the question of whether further increasing the charge q_{Cl_p} would improve the

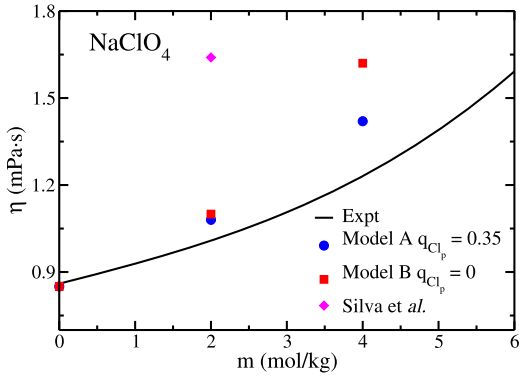

Fig. 2. Shear viscosity curves as a function of concentration for aqueous $NaClO_4$ solutions at 298.15 K and 1 bar. Model A with $q_{Cl_p} = 0.35e$ is depicted with blue circles whereas model B with $q_{Cl_p} = 0e$, with red squares. Magenta diamond is obtained from the work of da Silva et al. [92] (using a force field with a net charge of -1e for the ClO_4^{-1} anion, with $q_{Cl_p} = 1.08e$ and using TIP4P/2005 for water). The continuous line is the fit of the experimental data taken from Ref. [93].

agreement with the experimental viscosity even more. This is not the case. Increasing the charge to $q_{Cl_p} = 1e$ (this model will be denoted as Model C) increases the viscosity again (results for Model C are presented in the Supplementary Material). Thus, the viscosity presents a minimum as a function of q_{Cl_p} and the value of Model A (i.e., $q_{Cl_p} = 0.35e$) seems indeed an optimal choice. In Fig. 2 results are presented for the viscosity from the force field of Silva et al. [92] which also uses TIP4P/2005 for water. As can be seen, this model significantly overestimates the experimental viscosity. This is due to two reasons: the net charge of the perchlorate anion is -1e (and not -0.85e as in the Madrid-2019 force field) and the value of the charge $q_{Cl_p} = 1.08e$ is high. These two factors contribute to a significantly high value of the viscosity.

Based on these results, we decided to further investigate the effect of charge distribution in divalent salts (i.e., $Mg(ClO_4)_2$ and $Ca(ClO_4)_2$). To the best of our knowledge, no experimental viscosity data for these salts have been published, so we measured them in this study. The experimental data are collected in Table IV. In Fig. 3(a), we show the results for these two salts up to concentrations of ~4 m. As with the chloride salts [65], we observe that for perchlorates, the magnesium salt exhibits higher viscosities than the calcium perchlorate. In Fig. 3(b), we compare the experimental results for $Ca(ClO_4)_2$ with our simulation data. Similar to the behavior seen with $NaClO_4$, both models tend to overestimate the experimental data, but model A shows better agreement with the experimental values.

Table IV
Experimental (η^{Expt}) and simulation results (η^A for model A and η^B for model B) measured and computed in this work for the viscosity variation with molality for $Mg(ClO_4)_2$ and $Ca(ClO_4)_2$ aqueous solutions at 1 bar and 298.15 K. Simulation results for $Ca(ClO_4)_2$ were computed at 4 m.

$Mg(ClO_4)_2$		$Ca(ClO_4)_2$			
Expt		Expt		Sim	
m (mol/kg)	η^{Expt} (mPa·s)	m (mol/kg)	η^{Expt} (mPa·s)	η^A	η^B
1.213	1.246	1.000	1.075		
2.000	1.615	2.001	1.376		
3.797	3.148	3.993	2.535	3.65	4.40

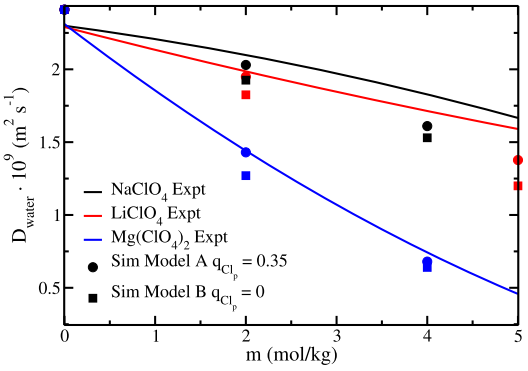

Fig. 4. Self diffusion coefficients of water as a function of concentration for aqueous $NaClO_4$ (black), $LiClO_4$ (red) and $Mg(ClO_4)_2$ (blue) solutions at 298.15 K and 1 bar. Model A with $q_{Cl_p} = 0.35e$ is depicted with circles whereas model B with $q_{Cl_p} = 0e$, with squares. The results include hydrodynamic corrections of Yeh and Hummer. [83] The continuous lines are fit of the experimental data taken from Ref. [94].

Regarding other transport properties, the diffusion coefficients of water have also been computed for both developed models. In Fig. 4, we present the diffusion coefficient of water as a function of electrolyte molality for $LiClO_4$, $NaClO_4$, and $Mg(ClO_4)_2$. It can be observed that in all cases, the experimental diffusion coefficients of water (solid lines) decrease as a function of concentration, with the decrease being more pronounced for $Mg(ClO_4)_2$ than for $LiClO_4$ and $NaClO_4$, which are quite similar (with sodium being slightly higher). The developed models are able to (1) correctly capture the trend of decreasing diffusion as a function of the salt, and (2) provide excellent simulation results in comparison with experimental data. It is worth noting that the results from model A are slightly higher (and thus closer to the experimental values)

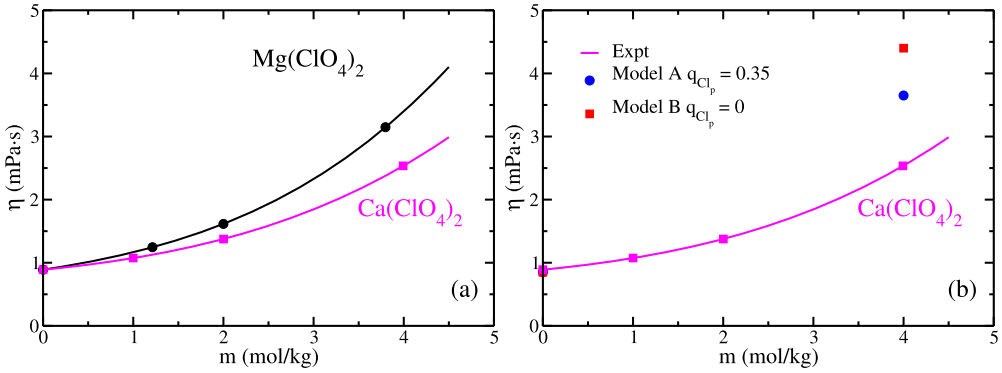

Fig. 3. (a) Experimental shear viscosity curves as a function of concentration for aqueous $Mg(ClO_4)_2$ (black solid line) and $Ca(ClO_4)_2$ (magenta line) solutions at 298.15 K and 1 bar. (b) Simulation results for viscosities using Model A with $q_{Cl_p} = 0.35e$ (blue circles) and model B with $q_{Cl_p} = 0e$ (red squares).

Table V
Self-diffusion coefficients of the ClO_4^- anion in aqueous solutions of $NaClO_4$, at 25 °C and 1 bar as a function of molality. Results include the hydrodynamic corrections of Yeh and Hummer. [83] At 0 m the data have been extrapolated. Experimental diffusion coefficients were taken from Ref. [94].

	$D_{ClO_4^-} \cdot 10^9$ (m^2s^{-1})		
m (mol/kg)	Model A	Model B	Expt
1	1.32	1.21	1.44
0.5	1.51	1.32	1.58
0	1.71	1.44	1.792

than those from model B. This is consistent with the lower viscosity observed for model A in Fig. 2.

Finally, we have calculated the diffusion coefficients of the perchlorate anion at infinite dilution ($D^{\infty}_{ClO_4^-}$). To compute it, we have calculated the diffusion coefficients (including the Yeh and Hummer corrections) of the perchlorate anion at 1 and 0.5 m and extrapolated to 0 m (i.e., infinite dilution), these results are collected in Table V. The experimental diffusion coefficient of this anion [94] is $D^{\infty,Expt}_{ClO_4^-} = 1.792 \cdot 10^{-9}$ m^2s^{-1}. The calculated $D^{\infty,sim}_{ClO_4^-}$ for model A and B are 1.71 and 1.44 $\cdot 10^{-9}$ m^2s^{-1} respectively. As expected, model A gives higher values for D than model B. Besides, the diffusion coefficient at infinite dilution of perchlorate anion by using model A is very similar to the experimental one (1.79 *vs* 1.71).

4.3. Temperatures of maximum in density and supercooled regime

Another interesting property that serves as an indicator of the performance of the force field is the temperature of maximum density (TMD). It is well known that water exhibits a maximum in density as a function of temperature at 4 °C [95] that is related to its overall structure [96]. When adding salt this TMD decreases due to the addition of the electrolyte [41,87,97–101]. The maximum in density is therefore often located in the supercooled region of water, making experimental measurements of these solutions challenging. Additionally, due to the low temperatures, simulations require long run times (between 300–600 ns for 1 m solutions) to accurately determine the TMD of aqueous solutions. In the last years we have computed by molecular dynamics simulations and experimentally measured the TMDs of a wide variety of aqueous solutions ranging for monovalent and divalent salts [87,99], salts with more complex ions such as ammonium and nitrate [102] or even bases like NaOH and KOH [67].

In most cases, we observed good agreement between simulations and experiments when using a scaled charge of ±0.85*e* for the ions. This means that the effect of ions in the solutions is well captured, taking into account that the TMD of the water model TIP4P/2005 (277.3 K) is in excellent agreement with the experimental value (277 K) [103]. In sharp contrast, unit charges tended to underestimate the TMD, while a charge of ±0.75*e* (which successfully reproduced transport properties) overestimated the TMD. However, the case of the NO_3^- ion was somewhat different, as a charge of ±0.85*e* consistently underestimated the experimental TMD. This suggests that charge distribution, which appeared to influence viscosity, may also play a role in determining the TMD. Although further studies would be valuable to better understand the effect of charge distribution in nitrate salts, the present work—featuring two different charge distributions for the perchlorate anion—serves as a representative example of this phenomenon.

In Fig. 5, we have plotted the densities of $Mg(ClO_4)_2$ and $Ca(ClO_4)_2$ as a function of temperature. Dashed lines represent the experimental measurements from this work for $Mg(ClO_4)_2$ (orange) and $Ca(ClO_4)_2$ (black), with the TMD in each case depicted as a filled triangle. As observed in previous studies [87,99], calcium provokes a larger shift in the TMD than magnesium, with the TMD of the latter being approxi-

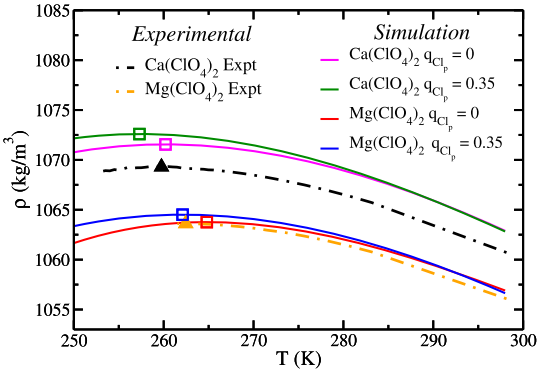

Fig. 5. Results (at 1 bar) for temperatures of maximum density for 0.4 m $Mg(ClO_4)_2$ and $Ca(ClO_4)_2$ solutions. The dashed lines are fits of the experimental data measured in this work for $Mg(ClO_4)_2$ (orange) and $Ca(ClO_4)_2$ (black). Experimental TMD is showed as a filled up triangle. Solid lines are fits of the simulation results by using model A with $q_{Cl_p} = 0.35e$ for $Mg(ClO_4)_2$ (blue) and $Ca(ClO_4)_2$ (green) and by using model B with $q_{Cl_p} = 0e$ for $Mg(ClO_4)_2$ (red) and $Ca(ClO_4)_2$ (magenta). Simulation TMD is showed as an empty square. Densities (both from experiment and from simulations) are explicitly provided in the Supplementary Material).

Table VI
Temperatures of maximum in density (TMD) and densities at the TMD (ρ_{max}) for 0.4 m aqueous solutions of $Mg(ClO_4)_2$ and $Ca(ClO_4)_2$, at 1 bar for models A and B and for experiments. Simulation and experimental results have been obtained in this work.

	Model A	Model B	Expt
$Mg(ClO_4)_2$ 0.4 m			
TMD (K)	262.1	264.8	262.5
ρ_{max} (kg/m^3)	1064.5	1063.8	1063.6
$Ca(ClO_4)_2$ 0.4 m			
TMD (K)	257.3	260.2	259.8
ρ_{max} (kg/m^3)	1072.6	1071.55	1069.3

mately 3 K higher than that of the former (~263 K *vs.* ~260 K). Using the experimental values of Despretz constant published in Ref. [99], we estimate a Despretz constant for perchlorate anion of $K_m^{ClO_4^-}$ = -13.5 K·kg·mol^{-1}, slightly lower than that of the other polyatomic anion SO_4^{2-} (-15.8 K·kg·mol^{-1}) [99].

Regarding the simulation results (solid lines), we first analyze the effect of charge distribution before comparing with experiments (all the simulation and experimental results are collected in Table VI). Model A, which features a greater difference in charges between Cl_p and O_p atoms, consistently predicts a lower TMD than Model B, where the partial charges are more similar. This suggests that decreasing the charge on the central atom (Cl_p), thereby making the partial charges of the molecule atoms more similar, leads to an increase in the TMD. To check that, we have also employed a force field for $Mg(ClO_4)_2$ with the same LJ parameters as the others, but assigning a charge of $q_{Cl_p} = 1e$ (model C previously presented). The results can be found in the Supplementary Material (Fig. S1 and Table SXI), and it can be observed that the increasing charge over the chlorine atom shifts the TMD to lower values deviating significantly from the experimental results. Concerning the TMD both models A and B are quite reasonable and provide quite good estimates of the location of the TMD (model B predicts slightly better the density at the maximum and model A predicts slightly better the temperatures at the maximum). Thus, concerning densities and TMD predictions models A and B perform quite well. It is only when considering transport properties that Model A performs better. For this reason from the results of this work our recommendation for simulating the perchlorate anion is to use Model A.

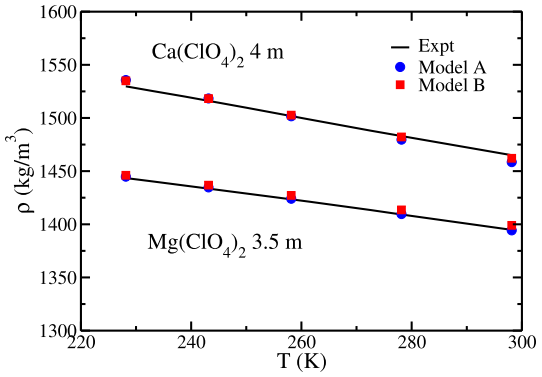

Fig. 6. Results (at 1 bar) for densities as a function of temperature for 3.5 m $Mg(ClO_4)_2$ and 4 m $Ca(ClO_4)_2$ solutions. The solid lines are fits of the experimental data measured in this work. Blue circles and red squares are the simulation results of this work using models A and B respectively.

Both models A and B describe reasonably well the TMD. Let us start by the $Ca(ClO_4)_2$, in this case it is evident that model B with $q_{Cl_p} = 0e$ (magenta empty square) provides results in better agreement with experiments than model A with $q_{Cl_p} = 0.35e$ (green empty square). On the other hand, for $Mg(ClO_4)_2$ this discussion is more difficult, given that the location of TMD is better predicted by model A (blue empty square) but the density at the maximum is excellently reproduced by model B (red empty square). Thus, this choice is difficult, and as we will point out at the end of this work, the answer to the charge distribution will depend on the studied property. We leave the final decision to the reader.

As one of the main interests in perchlorate salts lies in their presence on the surface of Mars, where extremely low temperatures prevail, we have evaluated the performance of our force field under such conditions. In fact, the temperature of maximum density (TMD) is already a good indicator of the performance of the model in the low-temperature regime, as it lies within the supercooled region.

Nevertheless, exploring even lower temperatures is relevant to test the broader applicability of our model. To this end, we have experimentally measured (see Experimental Procedure section) the densities of $Mg(ClO_4)_2$ and $Ca(ClO_4)_2$ at 3.5 and 4 m, respectively. In both cases, temperatures as low as 228.15 K (–45 °C) were reached, thus extending the applicability of our model into this range.

Subsequently, we performed simulations of both models (A and B) at these low temperatures. As shown in Fig. 6, both models accurately reproduce the experimental densities, with model A performing slightly better for $Mg(ClO_4)_2$ and model B for $Ca(ClO_4)_2$. The experimental and simulated density values are collected in Table VII.

In conclusion, the developed models are capable of reliably reproducing the densities of magnesium and calcium perchlorates at low temperatures comparable to those found on the Martian surface, at least within the 228–298 K range.

4.4. Structural features

The characterization of structural features in aqueous perchlorate solutions is also of interest, although experimental studies on this topic are scarce. Among the few available studies, the O_w-O_p distance is reported to be 3.07 Å in an IR study [104] and in the range of 2.4-3.2 Å based on neutron diffraction [105]. The radial distribution functions (RDFs) for O_w-Cl_p, O_w-O_p, and Na-Cl_p calculated with molecular dynamic simulations for both models A (blue solid line) and B (red solid line) are presented in Fig. 7 (a), (b), and (c), respectively. The overall structure is similar for both models, though some differences can be observed.

In Fig. 7(a), where the O_w-Cl_p RDF is plotted, two distinct maxima are observed in both models. These peaks are caused by the penetration of water molecules into the tetrahedral structure of the perchlorate (the first peak at 3.84 Å and 3.68 Å for models A and B, respectively) and the water molecules located outside the tetrahedron (the second peaks at 4.62 Å and 4.48 Å for models A and B, respectively). Notably, the model with $q_{Cl_p} = 0$ allows water molecules to penetrate more easily (resulting in shorter distances) due to the reduced electrostatic repulsion between O_p and O_w. By integrating these RDFs up to 5 Å we estimate a hydration of approximately 15 water molecules around the perchlorate anion in both models being 15.3 for model A and 14.8 for model B.

Regarding the O_w-O_p RDF (see Fig. 7(b)), we find the same O_w-O_p distance for both models, which is 3.28 Å. This value is close—although slightly larger—to the experimental distances reported previously [104,105]. Finally, from the Na-Cl_p RDFs presented in Fig. 7(c), the existence of contact ion pairs (CIP) can be observed. By integrating both RDFs up to their first minimum, we obtain a similar CIP value of approximately 0.3 for both models. However, some differences can be observed in the Na-Cl_p RDF, with model A showing a slightly larger Na-Cl_p distance than model B (3.30 Å *vs.* 3.06 Å). This can be easily explained by the fact that chloride in model A has a partial charge of +0.35*e*, which leads to electrostatic repulsion between Na and Cl_p, increasing the distance slightly. In contrast, in model B, where $q_{Cl_p} = 0e$, this electrostatic repulsion is absent, and only the Lennard-Jones interaction plays a role.

Table VII
Experimental (ρ^{Expt}) and simulation results (ρ^A for model A and ρ^B for model B) measured and computed in this work for the density variation with temperature for 3.5 m $Mg(ClO_4)_2$ and 4 m $Ca(ClO_4)_2$ aqueous solutions at 1 bar.

	$Mg(ClO_4)_2$ 3.5 m			$Ca(ClO_4)_2$ 4 m		
T (K)	ρ^{Expt} (kg/m^3)	ρ^A	ρ^B	ρ^{Expt} (kg/m^3)	ρ^A	ρ^B
298.15	1394.8	1394.3	1399.0	1465.0	1458.5	1462.1
278.15	1409.2	1409.6	1413.5	1483.0	1479.6	1482.1
273.15	1412.9			1487.5		
268.15	1416.5			1492.4		
263.15	1420.1			1497.0		
258.15	1423.7	1424.0	1427.1	1501.6	1501.6	1502.7
253.15	1426.8			1506.5		
248.15	1430.2			1511.5		
243.15	1433.6	1434.7	1436.8	1516.2	1518.4	1518.2
238.15	1436.9			1520.8		
233.15	1440.2			1525.2		
228.15	1443.5	1444.8	1446.1	1529.8	1535.6	1534.9

4.5. Compatibility with TIP4P/Ice water model

In a recent study, we presented a simple recipe to combine the TIP4P/Ice model, specifically designed for modeling ices and hydrates, with the Madrid-2019 force field for ions, initially developed in combination with the TIP4P/2005 water model [106]. This combination was motivated by the interest in modeling the freezing point depression of ice (or the T_3 decrease as a function of salt molality in the case of gas hydrates) using accurate force fields for both water and ions. Thus, the TIP4P/Ice model, with a melting point of 270 K [107,108], and the Madrid-2019 force field, which excellently captures the shift in the melting point [37] and in T_3 [39] of ices and hydrates, were selected.

The presence of magnesium and calcium perchlorates on Martian soil and subsoil, along with the deep eutectic points of both salts, makes the study of freezing point depression for these salts of particular interest. While this is beyond the scope of the present work, one optimal model combination for such research would be the aforementioned Madrid-2019 + TIP4P/Ice. In this study, we present the densities of various perchlorate salts at intermediate concentrations using the proposed model combination. As shown in Fig. 8 the results closely match experimental data (solid lines) and align well with those obtained using the originally developed model in combination with the TIP4P/2005 water model.

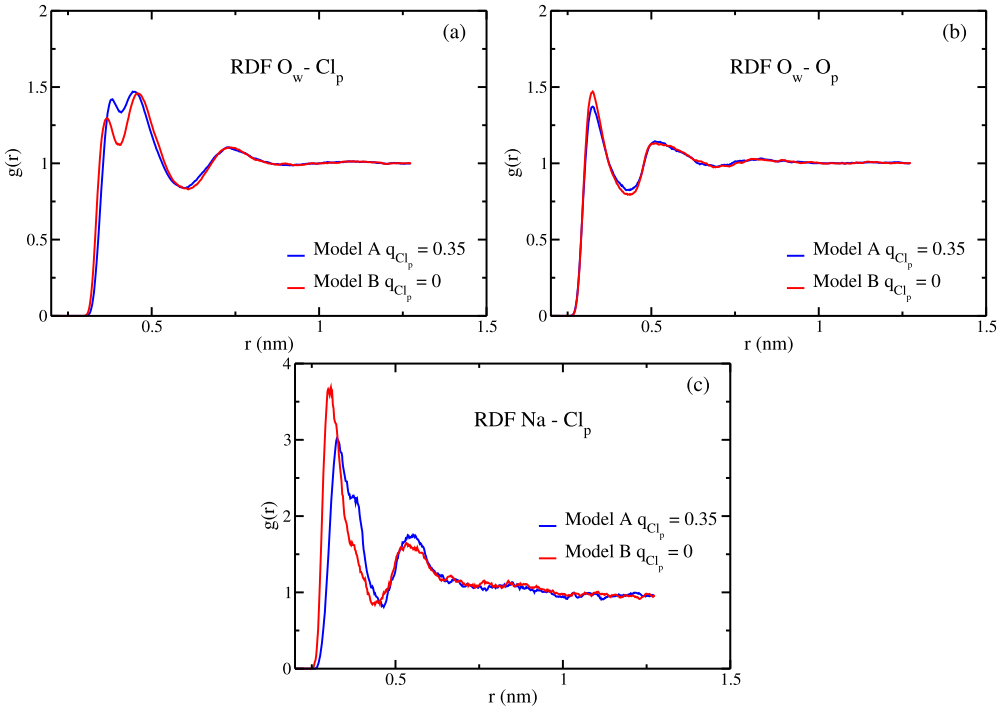

Fig. 7. Structural features of perchlorate solutions. (a) O_w-Cl_p (b) O_w-O_p and (c) Cl_p-Na radial distribution functions for 1 m $NaClO_4$ solutions at 298.15 K and at 1 bar obtained with the models A (blue) and B (red) developed in this work.

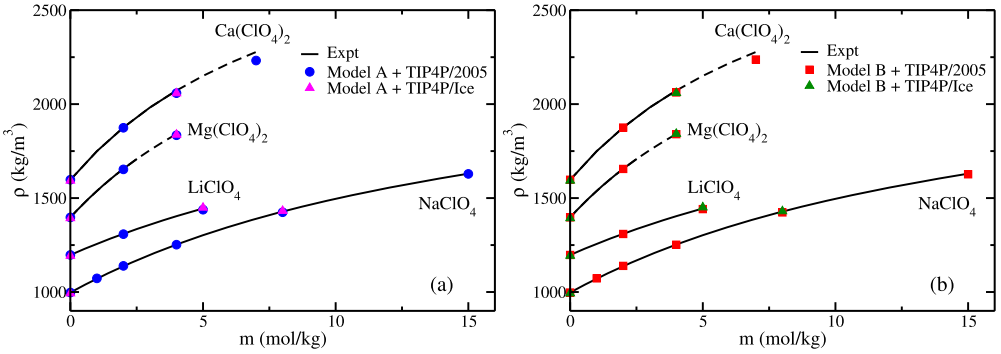

Fig. 8. Density as a function of molality at T = 298.15 K and 1 bar for different perchlorate aqueous solutions. (a) Results for model A. (b) Results for model B. Blue circles and red squares are the simulation results of this work using models A and B + TIP4P/2005 water respectively. Magenta and green up triangles are the simulation results of this work using models A and B + TIP4P/Ice water respectively. Solid black lines: fit of experimental data taken from Ref. [89] for $LiClO_4$, from Ref. [90] for $NaClO_4$ and $Ca(ClO_4)_2$ and from Ref. [91] for $Mg(ClO_4)_2$. Results for $LiClO_4$, $Mg(ClO_4)_2$ and $Ca(ClO_4)_2$ were shifted up 200, 400 and 600 density units respectively for a better legibility.

Nevertheless, one can say that density is primarily determined by the σ parameters of the Lennard-Jones potential which are the same in both combinations, and thus we cannot ensure the validity of the combination with the TIP4P/Ice model for other properties. For that reason, we have studied the viscosities of 2 m and 4 m $NaClO_4$ aqueous solutions. This study was carried out at room temperature and pressure, due to the lack of available experimental data for transport properties at low temperatures.

As we showed in our previous work [106], the viscosity of pure water using TIP4P/Ice model is nearly twice that of TIP4P/2005. Therefore, transport properties should not be calculated using this combination. In Fig. 9(a), we now show the viscosities obtained using model A in combination with TIP4P/Ice water. As expected, the absolute viscosities are significantly higher than those obtained with TIP4P/2005 water. However, in Fig. 9(b) we plot the change in viscosity η-η_0 (i.e., the difference between the viscosity of the model at each concentration and the viscosity of the model for pure water). It can be seen that this difference does not change dramatically, ensuring that the effect of ions in the solution is quite similar.

In any case, while we recommend using the perchlorate model in combination with TIP4P/2005 for simulations at room temperature and for studying transport properties, the combination with TIP4P/Ice is more appropriate at lower temperatures, particularly for studying freezing point depression, as the melting temperature of TIP4P/Ice is closer to the experimental value. Indeed, TIP4P/Ice has a melting point of 270 K, (20 K higher than that of TIP4P/2005 (250 K)), and the system dynamics are faster at higher temperatures. Therefore, although the TIP4P/Ice combination yields higher viscosities, it would be simulated at a temperature 20 K higher for the same degree of supercooling. This results in comparable dynamics to those obtained with the perchlorate force field in combination with TIP4P/2005.

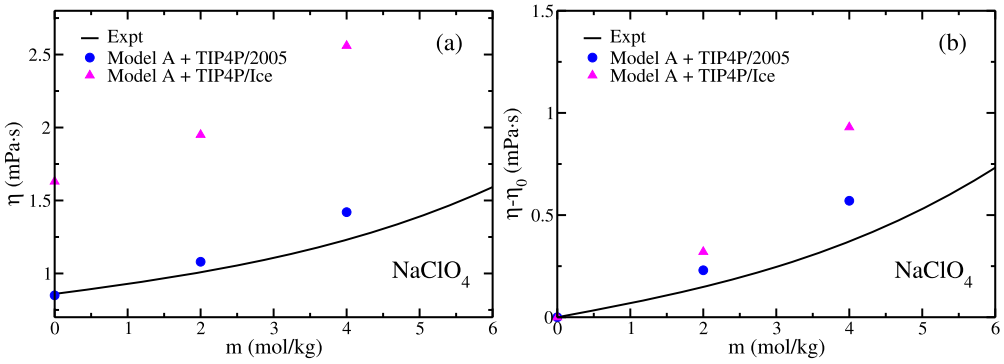

Fig. 9. (a) Viscosity (η) as a function of molality at T = 298.15 K and 1 bar for $NaClO_4$ aqueous solutions at different concentrations. (b) Difference between the viscosity at each concentration (η) and the viscosity of pure water for each model (η_0) as a function of concentration for aqueous $NaClO_4$ solutions at 298.15 K and 1 bar. Blue circles are the simulation results of this work using model A + TIP4P/2005 water. Magenta up triangles are the simulation results of this work using model A and TIP4P/Ice water. Solid black lines: fit of experimental data taken from Ref. [93].

Thus, in principle, the model can be used in future studies of freezing depression by combining the Madrid-2019 force field and the TIP4P/Ice model of water, although for other properties of aqueous solutions, as mentioned in this text, it is more appropriate to use TIP4P/2005.

5. Conclusions

In this work, we have developed a force field for the perchlorate anion (ClO_4^-) using a scaled charge of -0.85, in combination with the previously developed cations from the Madrid-2019 force field [65,66,77,78]. We propose two different charge distributions (i.e., two models) for the perchlorate anion. In Model A, the charge assigned to the Cl_p atom is $q = +0.35e$ (thus, the charges on the O_p atoms are $q = -0.30e$), and in Model B, the charge on the Cl_p atom is $q = 0e$ (thus the charges on the O_p atoms are $q = -0.2125e$). The Lennard-Jones parameters are the same for both models, but the charge distribution influences several studied properties. We have adjusted the models to reproduce the experimental densities of several soluble perchlorate salts, namely $LiClO_4$, $NaClO_4$, $KClO_4$, $Mg(ClO_4)_2$, and $Ca(ClO_4)_2$, up to the solubility limit of each salt.

Once the densities were reproduced by both models, we studied the effect of charge distribution on transport properties. We found that both models overestimate the experimental viscosities, but Model A, with more disparate partial charges, provides lower viscosity values, demonstrating the impact of charge distribution on this property. This effect had been previously noted for other ions but it had not been studied in detail [55,65–67]. For diffusion coefficients, we also observed the influence of charge distribution, with the computed results for Model A being higher than those for Model B. However, in this case, the experimental diffusion coefficients are well-described by the simulation results of Model A.

The TMD of the developed models was also calculated at 0.4 m and compared with experimental data, which were also obtained. The comparison shows good agreement with the experiments, with Model B (with less disparate charges) performing slightly better. Additionally, structural features of these solutions were studied, revealing a hydration number of approximately 15 water molecules around the perchlorate anion for both models, a number of 0.3 contact ion pairs, and an O_w-O_p distance of 3.28 Å for both models, which is close to the experimental value of 3.07 Å reported by IR [104]. Finally, we tested the compatibility of the developed models with the TIP4P/Ice water force field for future studies on freezing depression. We observed excellent agreement between the simulated densities using the proposed model combined with TIP4P/Ice water and the experimental densities.

Taken together, the results of this work present a reliable force field for the perchlorate anion in aqueous solutions, which can be used for a wide range of studies, particularly given the increasing importance of perchlorate due to its presence on Mars and to the property of perchlorates to significantly lower the freezing temperature of water in solutions [11,14,15]. Additionally, we provide an extensive discussion on the effect of charge distribution in polyatomic ions, observing that mainly the TMD and transport properties are influenced by this factor.

Although more properties should be addressed to properly evaluate the overall performance of the two proposed models A and B (and the worse model C, presented in the Supplementary Material), given the results of this work, we suggest the use of model A for the perchlorate anion in combination with either TIP4P/2005 or TIP4P/Ice for water.

CRediT authorship contribution statement

S. Blazquez: Conceptualization, Writing – review & editing, Writing – original draft, Validation, Software, Methodology, Investigation, Formal analysis, Data curation. **J. Troncoso:** Writing – review & editing, Validation, Resources, Methodology, Investigation, Formal analysis, Data curation, Conceptualization. **P. La Francesca:** Writing – review & editing, Investigation, Formal analysis, Conceptualization. **P. Gallo:** Writing – review & editing, Funding acquisition, Project administration, Investigation, Conceptualization. **M.M. Conde:** Resources, Methodology, Project administration, Funding acquisition, Writing – review & editing, Supervision, Investigation, Conceptualization. **C. Vega:** Project administration, Investigation, Funding acquisition, Formal analysis, Supervision, Writing – review & editing, Writing – original draft, Conceptualization.

Declaration of competing interest

The authors declare that they have no known competing financial interests or personal relationships that could have appeared to influence the work reported in this paper.

Acknowledgements

This work was funded by Grants No. PID2022-136919NB-C31, PID2022-136919NB-C32 and PID2023-147148NB-I00 of the MICINN and PNRR-M4C2-I1.1-PRIN 2022-PE9-ARES - Assessing the origin and stability of Martian subglacial waters-F53D23001240006 - Funded by EU-NextGenerationEU. The authors gratefully acknowledge the Universidad Politecnica de Madrid (www.upm.es) for providing computing resources on Magerit Supercomputer.

Appendix A. Implementing the force field of ClO_4^- in MD programs

In this work the perchlorate anion is treated as a rigid body (i.e., all bond angles and distances are fixed and the anion exhibits a per-

fect tetrahedral geometry). Imposing a tetrahedral rigid geometry in MD runs may be tricky (in Monte Carlo codes it does not introduce any complexity). One possibility is to use quaternions to integrate the equations of motion for the rotation of the rigid molecules of the system (including the perchlorate anion). Quaternions are indeed incorporated in MD codes such as LAMMPS [109]. However, they are not found in other MD programs and besides they are used rarely nowadays. The second possibility is to implement the rigidity by using constraints on the bond lengths. This is the procedure used in this work. We have done that by imposing constraints on the six O_p-O_p distances (imposing the value 2.335 Å) and determining the position of Cl_p as the geometrical center of the four O_p positions. This guarantees the rigid tetrahedral geometry (with Cl_p-O_p distances of 1.43Å and O_p-O_p distances of 2.335Å). The six constraints on O_p-O_p bond lengths are implemented using the SHAKE algorithm [76] and Cl_p is treated as a dummy atom of zero mass whose mass has been distributed among the four oxygen atoms O_p of the perchlorate anion. This mass redistribution affects slightly the rotational dynamics of the perchlorate anion (it increases the inertia moment of the perchlorate anion and the rotational dynamics becomes slightly slower) but has almost no impact on the translational dynamics. Notice also that in classical statistical mechanics the thermodynamic properties (densities, enthalpies, TMD, freezing point depressions, radial distribution functions, etc) are not affected by the mass of the atoms of the system. Thus thermodynamic properties are not affected by this internal mass redistribution. The SHAKE algorithm [76] is implemented in LAMMPS and also in versions of GROMACS up to a few years ago. Therefore, the force field presented in this work can be implemented easily using either LAMMPS or some GROMACS versions. However, we would like to give another extra option for those MD codes without quaternions or without the SHAKE algorithm (or simply for users of GROMACS preferring the LINCS algorithm for constraints). For this purpose we have generated a new version of the force field where the condition of full rigidity is slightly relaxed. This is achieved by imposing constraints only to the Cl_p-O_p distances, and including intramolecular O_p-O_p interactions (in the rigid version intramolecular O_p-O_p interactions are not included but they should be considered in the flexible version of the force field in order to keep a tetrahedral flexible geometry). In this case one can use for instance LINCS [110] to constraint these four distances (or any other algorithm available for constraining bond lengths). The perchlorate now has a little bit of flexibility so that it has small deviations from the perfect tetrahedral geometry. In this alternative the O_p-O_p distances are left flexible, resulting in a slightly deformable, but on average tetrahedral, geometry. This geometry allows for a realistic mass distribution, avoiding the need to reassign the Cl_p mass to the oxygen atoms, also resulting in a less perturbed rotational dynamics. We shall denote this particular implementation as Flexible, and that using SHAKE and a perfect tetrahedral geometry as Rigid. Notice that with the Flexible version it is also possible to use a time step of 2 fs so that the Flexible version is not slower than the rigid one. We shall now discuss briefly the results for Model A, implemented with the "Rigid" and with the "Flexible" topologies for the densities, viscosities, and diffusion coefficients of water. Although results are shown for Model A, the Flexible approach can also be used with Model B. In the Supplementary material (first five Tables) the densities obtained when using the Flexible and Rigid implementations of Model A are compared. The differences were found to be quite small (smaller than 0.2% in all the cases). Thus, the equations of state of the Flexible and Rigid implementations are almost identical.

With respect to transport properties in Table VIII the diffusion coefficient of water at high concentrations is presented for the Rigid and Flexible versions of the force field (Model A). Again, the diffusion coefficients are quite similar in both cases for all the perchlorate aqueous solutions considered in this work.

Finally, we have also computed the viscosity for model A of $NaClO_4$ at 298.15 K, 1 bar and a concentration of 4 m using the Flexible and Rigid implementations of the force field. With the Flexible one we obtained 1.38(0.03) mPa·s, whereas with the Rigid we obtained 1.42(0.03) mPa·s, being the experimental value 1.23 mPa·s. Therefore, the two models (Rigid and Flexible) have almost identical viscosities, being slightly lower (but almost within the error bar) for the Flexible version and slightly closer to the experimental value.

Table VIII
Diffusion coefficient of water D_{wat} in several perchlorate ionic solutions using the rigid and flexible versions of the force field. Results were obtained for Model A at 1 bar and 298.15 K. The results include hydrodynamic corrections of Yeh and Hummer.

Salt	m (mol/kg)	D_{wat} ·10^9 (m^2s^{-1}) Flexible	Rigid
$LiClO_4$	5	1.35	1.34
$NaClO_4$	4	1.59	1.61
$Mg(ClO_4)_2$	4	0.73	0.68
$Ca(ClO_4)_2$	4	0.80	0.83

As a conclusion, both implementations of the force field, the Rigid and the Flexible, yield quite similar results for thermodynamic and transport properties and can be used with confidence. The user can select the most convenient implementation depending on the available software or any other physical reason.

Appendix B. Supplementary material

In the Supplementary Material we have collected the raw simulated and experimental data for densities, viscosities, diffusion coefficients of water and temperature of maximum in density. Comparison with model C is also shown in Supplementary Material. Besides, we provide the topology files for the developed models.

Supplementary material related to this article can be found online at https://doi.org/10.1016/j.molliq.2025.128035.

Data availability

The data that support the findings of this study are available within the article and in the Supplementary Material.

References

[1] G. Marion, D. Catling, K. Zahnle, M. Claire, Modeling aqueous perchlorate chemistries with applications to Mars, Icarus 207 (2010) 675–685.
[2] M.H. Hecht, S.P. Kounaves, R. Quinn, S.J. West, S.M. Young, D.W. Ming, D. Catling, B. Clark, W. Boynton, J. Hoffman, et al., Detection of perchlorate and the soluble chemistry of martian soil at the Phoenix lander site, Science 325 (2009) 64–67.
[3] B.L. Carrier, S.P. Kounaves, The origins of perchlorate in the martian soil, Geophys. Res. Lett. 42 (2015) 3739–3745.
[4] R.C. Quinn, H.F. Martucci, S.R. Miller, C.E. Bryson, F.J. Grunthaner, P.J. Grunthaner, Perchlorate radiolysis on Mars and the origin of martian soil reactivity, Astrobiology 13 (2013) 515–520.
[5] S.P. Kounaves, B.L. Carrier, G.D. O'Neil, S.T. Stroble, M.W. Claire, Evidence of martian perchlorate, chlorate, and nitrate in Mars meteorite eeta79001: implications for oxidants and organics, Icarus 229 (2014) 206–213.
[6] D. Catling, M. Claire, K. Zahnle, R. Quinn, B. Clark, M. Hecht, S. Kounaves, Atmospheric origins of perchlorate on Mars and in the Atacama, J. Geophys. Res. Planets 115 (2010) E0011.
[7] B.C. Clark, S.P. Kounaves, Evidence for the distribution of perchlorates on Mars, Int. J. Astrobiol. 15 (2016) 311–318.
[8] A.F. Davila, D. Willson, J.D. Coates, C.P. McKay, Perchlorate on Mars: a chemical hazard and a resource for humans, Int. J. Astrobiol. 12 (2013) 321–325.
[9] D.P. Glavin, C. Freissinet, K.E. Miller, J.L. Eigenbrode, A.E. Brunner, A. Buch, B. Sutter, P.D. Archer Jr, S.K. Atreya, W.B. Brinckerhoff, et al., Evidence for perchlorates and the origin of chlorinated hydrocarbons detected by Sam at the rocknest aeolian deposit in Gale crater, J. Geophys. Res. Planets 118 (2013) 1955–1973.
[10] O. Pestova, L. Myund, M. Khripun, A. Prigaro, Polythermal study of the systems m (ClO_4) 2-H_2O (M^{2+} = Mg^{2+}, Ca^{2+}, Sr^{2+}, Ba^{2+}), Russ. J. Appl. Chem. 78 (2005) 409–413.
[11] J. Toner, D. Catling, B. Light, The formation of supercooled brines, viscous liquids, and low-temperature perchlorate glasses in aqueous solutions relevant to Mars, Icarus 233 (2014) 36–47.
[12] P.H. Smith, L. Tamppari, R. Arvidson, D. Bass, D. Blaney, W.V. Boynton, A. Carswell, D. Catling, B. Clark, T. Duck, et al., H2o at the Phoenix landing site, Science 325 (2009) 58–61.

[13] N.O. Rennó, B.J. Bos, D. Catling, B.C. Clark, L. Drube, D. Fisher, W. Goetz, S.F. Hviid, H.U. Keller, J.F. Kok, et al., Possible physical and thermodynamical evidence for liquid water at the Phoenix landing site, J. Geophys. Res. Planets 114 (2009) E0003.
[14] R. Orosei, S.E. Lauro, E. Pettinelli, A. Cicchetti, M. Coradini, B. Cosciotti, F. Di Paolo, E. Flamini, E. Mattei, M. Pajola, et al., Radar evidence of subglacial liquid water on Mars, Science 361 (2018) 490–493.
[15] S.E. Lauro, E. Pettinelli, G. Caprarelli, L. Guallini, A.P. Rossi, E. Mattei, B. Cosciotti, A. Cicchetti, F. Soldovieri, M. Cartacci, et al., Multiple subglacial water bodies below the south pole of Mars unveiled by new marsis data, Nat. Astron. 5 (2021) 63–70.
[16] P. La Francesca, P. Gallo, Supercooled solutions of sodium perchlorate in tip4p/2005 water: the effect of martian solutes on thermodynamics and structure, J. Chem. Phys. 159 (2023) 124501.
[17] P. La Francesca, P. Gallo, Phase diagram and structure of tip4p/2005 water and magnesium perchlorate: a molecular dynamic study of martian aqueous solutions, J. Mol. Liq. 417 (2025) 126673.
[18] E.T. Urbansky, Perchlorate as an environmental contaminant, Environ. Sci. Pollut. Res. 9 (2002) 187–192.
[19] W.E. Motzer, Perchlorate: problems, detection, and solutions, Environ. Forensics 2 (2001) 301–311.
[20] G. Charnley, Perchlorate: overview of risks and regulation, Food Chem. Toxicol. 46 (2008) 2307–2315.
[21] R. Srinivasan, G.A. Sorial, Treatment of perchlorate in drinking water: a critical review, Sep. Purif. Technol. 69 (2009) 7–21.
[22] H. Laurent, A.K. Soper, L. Dougan, Trimethylamine n-oxide (tmao) resists the compression of water structure by magnesium perchlorate: terrestrial kosmotrope vs. martian chaotrope, Phys. Chem. Chem. Phys. 22 (2020) 4924–4937.
[23] F. Cao, J. Jaunat, N. Sturchio, B. Cances, X. Morvan, A. Devos, V. Barbin, P. Ollivier, Worldwide occurrence and origin of perchlorate ion in waters: a review, Sci. Total Environ. 661 (2019) 737–749.
[24] S. Susarla, T. Collette, A. Garrison, N. Wolfe, S. McCutcheon, Perchlorate identification in fertilizers, Environ. Sci. Technol. 33 (1999) 3469–3472.
[25] J. Wolff, Perchlorate and the thyroid gland, Pharmacol. Rev. 50 (1998) 89–105.
[26] National Research Council; Division on Earth and Life Studies; Board on Environmental Studies and Toxicology; Committee to Assess the Health Implications of Perchlorate Ingestion, Health Implications of Perchlorate Ingestion, National Academies Press, 2005.
[27] P. Niziński, A. Błażewicz, J. Kończyk, R. Michalski, Perchlorate–properties, toxicity and human health effects: an updated review, Rev. Environ. Health 36 (2021) 199–222.
[28] E. Sebastián, C. Armiens, J. Gómez-Elvira, M.P. Zorzano, J. Martinez-Frias, B. Esteban, M. Ramos, The rover environmental monitoring station ground temperature sensor: a pyrometer for measuring ground temperature on Mars, Sensors 10 (2010) 9211–9231.
[29] J.C. Hey, L.C. Smeeton, M.T. Oakley, R.L. Johnston, Isomers and energy landscapes of perchlorate–water clusters and a comparison to pure water and sulfate–water clusters, J. Phys. Chem. A 120 (2016) 4008–4015.
[30] K. Nieszporek, P. Podkościelny, J. Nieszporek, Transitional hydrogen bonds in aqueous perchlorate solution, Phys. Chem. Chem. Phys. 18 (2016) 5957–5963.
[31] V.N. Agieienko, Y.V. Kolesnik, O.N. Kalugin, Structure, solvation, and dynamics of Mg^{2+}, Ca^{2+}, Sr^{2+}, and Ba^{2+} complexes with 3-hydroxyflavone and perchlorate anion in acetonitrile medium: a molecular dynamics simulation study, J. Chem. Phys. 140 (2014) 194501.
[32] G. Heinje, W. Luck, K. Heinzinger, Molecular dynamics simulation of an aqueous sodium perchlorate solution, J. Phys. Chem. 91 (1987) 331–338.
[33] M. Baaden, F. Berny, C. Madic, G. Wipff, M3+ lanthanide cation solvation by acetonitrile: the role of cation size, counterions, and polarization effects investigated by molecular dynamics and quantum mechanical simulations, J. Phys. Chem. A 104 (2000) 7659–7671.
[34] I.-C. Yeh, G.M. Tow, Force field parameters for ammonium perchlorate validated using surface energies and applied to interactions with polymer binder, J. Phys. Chem. C 127 (2023) 18598–18608.
[35] M.D. Baer, I.-F.W. Kuo, H. Bluhm, S. Ghosal, Interfacial behavior of perchlorate versus chloride ions in aqueous solutions, J. Phys. Chem. B 113 (2009) 15843–15850.
[36] G.M. Tow, E.J. Maginn, Evaluating physical properties of the orthorhombic crystal phase of ammonium perchlorate using a class ii force field, J. Chem. Phys. 149 (2018) 244502.
[37] C.P. Lamas, C. Vega, E.G. Noya, Freezing point depression of salt aqueous solutions using the Madrid-2019 model, J. Chem. Phys. 156 (2022) 134503.
[38] S. Blazquez, I. Zeron, M. Conde, J. Abascal, C. Vega, Scaled charges at work: salting out and interfacial tension of methane with electrolyte solutions from computer simulations, Fluid Phase Equilib. 513 (2020) 112548.
[39] S. Blazquez, C. Vega, M. Conde, Three phase equilibria of the methane hydrate in nacl solutions: a simulation study, J. Mol. Liq. 383 (2023) 122031.
[40] M. Předota, D. Biriukov, Electronic continuum correction without scaled charges, J. Mol. Liq. 314 (2020) 113571.
[41] L. Perin, P. Gallo, Phase diagram of aqueous solutions of licl: a study of concentration effects on the anomalies of water, J. Phys. Chem. B 127 (2023) 4613–4622.
[42] G. Le Breton, L. Joly, Molecular modeling of aqueous electrolytes at interfaces: effects of long-range dispersion forces and of ionic charge rescaling, J. Chem. Phys. 152 (2020) 241102.
[43] M. Kohagen, P.E. Mason, P. Jungwirth, Accounting for electronic polarization effects in aqueous sodium chloride via molecular dynamics aided by neutron scattering, J. Phys. Chem. B 120 (2016) 1454–1460.
[44] E. Duboue-Dijon, M. Javanainen, P. Delcroix, P. Jungwirth, H. Martinez-Seara, A practical guide to biologically relevant molecular simulations with charge scaling for electronic polarization, J. Chem. Phys. 153 (2020) 050901.
[45] D. Biriukov, O. Kroutil, M. Předota, Modeling of solid–liquid interfaces using scaled charges: rutile (110) surfaces, Phys. Chem. Chem. Phys. 20 (2018) 23954–23966.
[46] S. Blazquez, J.L. Abascal, J. Lagerweij, P. Habibi, P. Dey, T.J. Vlugt, O.A. Moultos, C. Vega, Computation of electrical conductivities of aqueous electrolyte solutions: two surfaces, one property, J. Chem. Theory Comput. 19 (2023) 5380–5393.
[47] R. Savoj, H. Agnew, R. Zhou, F. Paesani, Molecular insights into the influence of ions on the water structure. i. Alkali metal ions in solution, J. Phys. Chem. B 128 (2024) 1953–1962.
[48] M. Jorge, Theoretically grounded approaches to account for polarization effects in fixed-charge force fields, J. Chem. Phys. 161 (2024) 180901.
[49] V. Kostal, P. Jungwirth, H. Martinez-Seara, Nonaqueous ion pairing exemplifies the case for including electronic polarization in molecular dynamics simulations, J. Phys. Chem. Lett. 14 (2023) 8691–8696.
[50] G. Cassinello, E.G. Noya, E. Sanz, C.P. Lamas, Phase diagram of nacl–water by computer simulations: performance of non-polarizable force-fields, Mol. Phys. 122 (2024) e2398133.
[51] S. Blazquez, M. Conde, C. Vega, Solubility of CO_2 in salty water: adsorption, interfacial tension and salting out effect, Mol. Phys. 122 (2024) e2306242.
[52] J. Han, Y. Gao, Y. Feng, Z. Yu, J. Wu, H. Fang, Toward mitigating the impact of non-bulk defects on describing water structure in salt aqueous solutions: characterizing solution density with a network-based structural indicator, J. Chem. Phys. 162 (2025) 024503.
[53] P. Habibi, A. Rahbari, S. Blazquez, C. Vega, P. Dey, T.J. Vlugt, O.A. Moultos, A new force field for OH^- for computing thermodynamic and transport properties of H_2 and O_2 in aqueous NaOH and KOH solutions, J. Phys. Chem. B 126 (2022) 9376–9387.
[54] W. Van Rooijen, P. Habibi, K. Xu, P. Dey, T. Vlugt, H. Hajibeygi, O. Moultos, Interfacial tensions, solubilities, and transport properties of the h2/h2o/nacl system: a molecular simulation study, J. Chem. Eng. Data 69 (2023) 307–319.
[55] P. Habibi, J.R. Postma, J.T. Padding, P. Dey, T.J. Vlugt, O.A. Moultos, Thermodynamic and transport properties of $H_2/H_2O/NaB(OH)_4$ mixtures using the delft force field (DFF/$B(OH)_4$-), Ind. Eng. Chem. Res. 62 (2023) 11992–12005.
[56] P. Habibi, P. Dey, T.J. Vlugt, O.A. Moultos, Effect of dissolved KOH and NaCl on the solubility of water in hydrogen: a Monte Carlo simulation study, J. Chem. Phys. 161 (2024) 054304.
[57] I. Leontyev, A. Stuchebrukhov, Electronic continuum model for molecular dynamics simulations, J. Chem. Phys. 130 (2009) 02B609.
[58] I.V. Leontyev, A.A. Stuchebrukhov, Electronic continuum model for molecular dynamics simulations of biological molecules, J. Chem. Theory Comput. 6 (2010) 1498–1508.
[59] I.V. Leontyev, A.A. Stuchebrukhov, Electronic polarizability and the effective pair potentials of water, J. Chem. Theory Comput. 6 (2010) 3153–3161.
[60] I. Leontyev, A. Stuchebrukhov, Accounting for electronic polarization in non-polarizable force fields 13 (2011) 2613–2626.
[61] Z. Kann, J. Skinner, A scaled-ionic-charge simulation model that reproduces enhanced and suppressed water diffusion in aqueous salt solutions, J. Chem. Phys. 141 (2014) 104507.
[62] Y. Yao, M.L. Berkowitz, Y. Kanai, Communication: modeling of concentration dependent water diffusivity in ionic solutions: role of intermolecular charge transfer, J. Chem. Phys. 143 (2015) 241101.
[63] Y. Yao, Y. Kanai, Free energy profile of NaCl in water: first-principles molecular dynamics with scan and wb97x-v exchange–correlation functionals, J. Chem. Theory Comput. 14 (2018) 884–893.
[64] S. Blazquez, M. Conde, C. Vega, Scaled charges for ions: an improvement but not the final word for modeling electrolytes in water, J. Chem. Phys. 158 (2023) 054505.
[65] I. Zeron, J.L.F. Abascal, C. Vega, A force field of Li^+, Na^+, K^+, Mg^2+, Ca^2+, Cl^-, and SO_4^{2-} in aqueous solution based on the TIP4P/2005 water model and scaled charges for the ions, J. Comput. Phys. 151 (2019) 134504.
[66] V.M. Trejos, M. de Lucas, C. Vega, S. Blazquez, F. Gámez, Further extension of the Madrid-2019 force field: parametrization of nitrate (NO_3^-) and ammonium (NH_4^+) ions, J. Chem. Phys. 159 (2023) 224501.
[67] M. de Lucas, S. Blazquez, J. Troncoso, C. Vega, F. Gámez, Dressing a nonpolarizable force field for OH^- in TIP4P/2005 aqueous solutions with corrected Hirshfeld charges, J. Phys. Chem. Lett. 15 (2024) 9411–9418.
[68] L. McFegan, Á. Juhász, P. Márton, Z. Horvolgyi, A. Jedlovszky-Hajdu, G. Hantal, P. Jedlovszky, Surface affinity of tetramethylammonium iodide in aqueous solutions: a combined experimental and computer simulation study, J. Phys. Chem. B 127 (2023) 5341–5352.
[69] D. van der Spoel, E. Lindahl, B. Hess, G. Groenhof, A.E. Mark, H.J.C. Berendsen, Gromacs: fast, flexible and free, J. Comput. Chem. 26 (2005) 1701.

[70] B. Hess, C. Kutzner, D. van der Spoel, E. Lindahl, Gromacs 4: algorithms for highly efficient, load-balanced, and scalable molecular simulation, J. Chem. Theory Comput. 4 (2008) 435–447.
[71] D. Beeman, Some multistep methods for use in molecular dynamics calculations, J. Comput. Phys. 20 (1976) 130–139.
[72] S. Nosé, A molecular dynamics method for simulations in the canonical ensemble, Mol. Phys. 52 (1984) 255–268.
[73] W.G. Hoover, Canonical dynamics: equilibrium phase-space distributions, Phys. Rev. A 31 (1985) 1695–1697.
[74] M. Parrinello, A. Rahman, Polymorphic transitions in single crystals: a new molecular dynamics method, J. Appl. Phys. 52 (1981) 7182–7190.
[75] U. Essmann, L. Perera, M.L. Berkowitz, T. Darden, H. Lee, L.G. Pedersen, A smooth particle mesh Ewald method, J. Chem. Phys. 103 (1995) 8577–8593.
[76] J.P. Ryckaert, G. Ciccotti, H.J. Berendsen, Numerical integration of the Cartesian equations of motion of a system with constraints: molecular dynamics of n-alkanes, J. Comput. Phys. 23 (1977) 327–341.
[77] S. Blazquez, M.M. Conde, J.L. Abascal, C. Vega, The Madrid-2019 force field for electrolytes in water using tip4p/2005 and scaled charges: extension to the ions F^-, Br^-, I^-, Rb^+, and Cs^+, J. Chem. Phys. 156 (2022) 044505.
[78] S. Blazquez, I.C. Bourg, C. Vega, Madrid-2019 force field: an extension to divalent cations Sr^{2+} and Ba^{2+}, J. Chem. Phys. 160 (2024) 046101.
[79] J.L.F. Abascal, C. Vega, A general purpose model for the condensed phases of water: Tip4p/2005, J. Chem. Phys. 123 (2005) 234505.
[80] M.M. Cox, J.W. Moore, The relative stabilities of perchlorate, perbromate, and periodate ions, J. Phys. Chem. 74 (1970) 627–631.
[81] M.M. Olmstead, Bond length of perchlorate at different temperatures: X-ray and neutron comparison, Cryst. Struct. Commun. 76 (2020) 159–163.
[82] J. Santos, P. Abreu, J. Marques, Calculation of diffusion coefficients of pesticides by employing molecular dynamics simulations, J. Mol. Liq. 340 (2021) 117106.
[83] I.C. Yeh, G. Hummer, System-size dependence of diffusion coefficients and viscosities from molecular dynamics simulations with periodic boundary conditions, J. Phys. Chem. B 108 (2004) 15873.
[84] M.A. González, J.L.F. Abascal, The shear viscosity of rigid water models, J. Chem. Phys. 132 (2010) 096101.
[85] W.M. Haynes, CRC Handbook of Chemistry and Physics, CRC Press, 2011.
[86] M. Souto-Caride, J. Troncoso, J. Peleteiro, E. Carballo, L. Romaní, Viscosity anomaly near the critical point in nitrobenzene + alkane binary systems, Phys. Rev. E 71 (2005) 041503.
[87] L.F. Sedano, S. Blazquez, E.G. Noya, C. Vega, J. Troncoso, Maximum in density of electrolyte solutions: learning about ion–water interactions and testing the Madrid-2019 force field, J. Chem. Phys. 156 (2022) 154502.
[88] L. Hnedkovsky, G. Hefter, Densities and apparent molar volumes of aqueous solutions of naclo4, kclo4, and kcl at temperatures from 293 to 343 k, J. Chem. Eng. Data 66 (2021) 3645–3658.
[89] B. Hu, L. Hnedkovsky, W. Li, G. Hefter, Densities and molar volumes of aqueous solutions of liclo4 at temperatures from 293 k to 343 k, J. Chem. Eng. Data 61 (2016) 1388–1394.
[90] A. Apelblat, A new two-parameter equation for correlation and prediction of densities as a function of concentration and temperature in binary aqueous solutions, J. Mol. Liq. 219 (2016) 313–331.
[91] R. Caro, L. Hnedkovsky, J.M. del Río, G. Hefter, Molar volumes and heat capacities of aqueous solutions of mg (clo4) 2, J. Chem. Eng. Data 65 (2020) 3735–3743.
[92] D.A. Da Silva, A. Messias, E.E. Fileti, A. Pascon, D.V. Franco, L.M. Da Silva, H.G. Zanin, et al., Effect of conductivity, viscosity, and density of water-in-salt electrolytes on the electrochemical behavior of supercapacitors: molecular dynamics simulations and in situ characterization studies, Mater. Adv. 3 (2022) 611–623.
[93] G.J. Janz, B. Oliver, G. Lakshminarayanan, G.E. Mayer, Electrical conductance, diffusion, viscosity, and density of sodium nitrate, sodium perchlorate, and sodium thiocyanate in concentrated aqueous solutions, J. Phys. Chem. 74 (1970) 1285–1289.
[94] S.R. Heil, M. Holz, T.M. Kastner, H. Weingärtner, Self-diffusion of the perchlorate ion in aqueous electrolyte solutions measured by 35 cl nmr spin–echo experiments, J. Chem. Soc., Faraday Trans. 91 (1995) 1877–1880.
[95] D. Eisenberg, W. Kauzmann, The Structure and Properties of Water, Oxford University Press, USA, 2005.
[96] J.R. Errington, P.G. Debenedetti, Relationship between structural order and the anomalies of liquid water, Nature 409 (2001) 318–321.
[97] National Research Council of USA, International Critical Tables of Numerical Data, Physics, Chemistry and Technology, in: E.W. Washburn, C.J. West (Eds.), McGraw-Hill, New York, 1928.
[98] J. Troncoso, D. González-Salgado, The temperature of maximum density for aqueous solutions, J. Chem. Phys. 160 (2024) 100902.
[99] F. Gámez, L.F. Sedano, S. Blazquez, J. Troncoso, C. Vega, Building a hofmeister-like series for the maximum in density temperature of aqueous electrolyte solutions, J. Mol. Liq. 377 (2023) 121433.
[100] D. Corradini, M. Rovere, P. Gallo, A route to explain water anomalies from results on an aqueous solution of salt, J. Chem. Phys. 132 (2010) 134508.
[101] D. Corradini, P. Gallo, Liquid–liquid coexistence in nacl aqueous solutions: a simulation study of concentration effects, J. Phys. Chem. B 115 (2011) 14161–14166.
[102] S. Blazquez, M. de Lucas, C. Vega, J. Troncoso, F. Gámez, The temperature of maximum in density of aqueous solutions of nitrate and ammonium salts: testing the Madrid-2019 force field, J. Chem. Phys. 161 (2024) 046103.
[103] L.F. Sedano, S. Blazquez, C. Vega, Accuracy limit of non-polarizable four-point water models: TIP4P/2005 vs OPC. Should water models reproduce the experimental dielectric constant?, J. Chem. Phys. 161 (2024) 044505.
[104] P.A. Bergstroem, J. Lindgren, O. Kristiansson, An IR study of the hydration of perchlorate, nitrate, iodide, bromide, chloride and sulfate anions in aqueous solution, J. Phys. Chem. 95 (1991) 8575–8580.
[105] G. Neilson, D. Schiöberg, W. Luck, The structure around the perchlorate ion in concentrated aqueous solutions, Chem. Phys. Lett. 122 (1985) 475–479.
[106] S. Blazquez, L.F. Sedano, C. Vega, On the compatibility of the Madrid-2019 force field for electrolytes with the tip4p/ice water model, J. Chem. Phys. 161 (2024) 224502.
[107] S. Blazquez, C. Vega, Melting points of water models: current situation, J. Chem. Phys. 156 (2022) 216101.
[108] M. Conde, M. Rovere, P. Gallo, High precision determination of the melting points of water tip4p/2005 and water tip4p/ice models by the direct coexistence technique, J. Chem. Phys. 147 (2017) 244506.
[109] A.P. Thompson, H.M. Aktulga, R. Berger, D.S. Bolintineanu, W.M. Brown, P.S. Crozier, P.J. In't Veld, A. Kohlmeyer, S.G. Moore, T.D. Nguyen, et al., Lammps-a flexible simulation tool for particle-based materials modeling at the atomic, meso, and continuum scales, Comput. Phys. Commun. 271 (2022) 108171.
[110] B. Hess, H. Bekker, H.J.C. Berendsen, J.G.E.M. Fraaije, Lincs: a linear constraint solver for molecular simulations, J. Comput. Chem. 18 (1997) 1463.